Lithium Titanate (LTO) Synthesis Through Solid State Reaction and Its Performance for $LiFePO_4$/LTO Battery

Viona Natalia[1], Anggia Putri Gustami[1], Fitria Rahmawati[1,3], Witri Wahyu Lestari[1] & Agus Purwanto[2,3]

[1]Research Group of Solid State Chemistry & Catalysis, Chemistry Department, Sebelas Maret University, Jl. Ir. Sutami 36 A, Kentingan, Surakarta 57126, Indonesia
[2]Chemical Engineering Department, Faculty of Engineering, Sebelas Maret University, Jl. Ir. Sutami 36 A, Kentingan Surakarta 57126, Indonesia
[3]National Centre for Sustainable Transportation Technology, Institut Teknologi Bandung, Jalan Ganesha 10, Bandung 40132, Indonesia
E-mail: fitria@mipa.uns.ac.id

Abstract. Lithium titanate, LTO, was synthesized by solid state reaction with Li_2CO_3 and TiO_2 powder as precursors. The result was characterized to investigate its crystal structure, phase content, cell parameters, surface morphology, electrical conductivity and its performance as electrode in a lithium ion battery. XRD analysis with Le Bail refinement showed that the prepared materials consisted of 4 phases of $Li_4Ti_5O_{12}$, Li_2TiO_3, anatase TiO_2 and rutile TiO_2. The surface morphology was still not homogeneous, with an average grain size of 0.533 ± 0.157 μm. When 1% LTO was mixed with graphite and used as anode of an LFP battery, it produced a specific capacity of 130.66 $mAhg^{-1}$ with Coulombic efficiency of 94.2%. When the composition was 5% of the total anode powder, the specific capacity was 118.74 $mAhg^{-1}$ and Coulombic efficiency was 92.72%.

***Keywords**: $LiFePO_4$; lithium-ion battery; lithium titanate; solid state reactions.*

1 Introduction

The use of fossil energy can be reduced by utilizing energy sources such as wind and sunlight. However, to ensure that this energy supply is sustainable, those energy sources need to be connected to energy storage such as batteries [1,2]. Batteries have the ability to store chemical energy that can be converted to electrical energy at a high conversion efficiency and without gas emission [3]. The rechargeable lithium-ion batteries (LiBs) have been widely developed because of their high energy density, long life cycle, and high battery efficiency [4]. Graphite is mostly used as the anode material due to its low cost, its abundance, and high theoretical specific capacity of 372 $mAhg^{-1}$ [5-7]. However, graphite can undergo volume expansion up to 10% during charging, which can cause severe structural destruction [8]. In addition, dendrites can be formed on the surface of graphite due to its low potential compared to lithium

Received November 6th, 2017, Revised February 23rd, 2018, Accepted for publication May 28th, 2018.
 ISSN: 2337-5760, DOI: 10.5614/j.math.fund.sci.2018.50.3.5

oxidation (about 0.2 V versus Li/Li^+). This may cause a short circuit or can lead to safety issues in LIB technology [9].

Lithium titanate, $Li_4Ti_5O_{12}$ (LTO), exhibits a high operation voltage, i.e. 1.55 V, compared to Li/Li^+, which can reduce the formation of dendrites on the surface of the electrode, improving the structure stability of the electrode [8-10]. Meanwhile, the theoretical specific capacity of LTO from spinel to rock salt is about 175m Ahg^{-1} [11]. LTO has low intrinsic electrical conductivity (ca. 10^{-13} $S.cm^{-1}$) and poor lithium-ion diffusivity (ca. 10^9-10^{13} $cm^2.S^{-1}$) [12,13]. Therefore, LTO needs modification to increase its electrical conductivity, for example by cation doping and conductive surface coating [11]. Previous research has succeeded in synthesizing an $Li_4Ti_5O_{12}$/silicon composite that showed good rate capability in the presence of LTO [12]. Meanwhile, the nitridated mesoporus $Li_4Ti_5O_{12}$ structure enhanced the electrical conductivity and rate capability [14]. Some methods used to synthesize LTO are hydrothermal [13], solvothermal, sol gel and solid state methods [15]. Solid state reaction is a simple method to produce a solid material without a specific instrument being required.

In this research, $Li_4Ti_5O_{12}$ was prepared by solid state reaction with two kinds of TiO_2 powder at different grades as starting material. The synthesis of LTO by solid state reaction usually uses Li source of LiOH but in this research the starting material was Li_2CO_3. By using Li_2CO_3, the formation of LTO will release CO_2 gas and leave an empty space for creating pores [16]. Meanwhile, LFP was used as the cathode because LFP has a high specific capacity of 170 $mAhg^{-1}$, is inexpensive and environmentally friendly [17]. For these reasons, LFP is widely used as cathode material in lithium ion batteries [18-20].

2 Experiment

2.1 Preparation of LTO

Lithium titanate was synthesized by solid state reaction with TiO_2 and Li_2CO_3 as precursors [21]. This research used two different commercial grades of anatase TiO_2, i.e. Merck, p.a. ICSD#24276 (TiO_2-A) and TOSOH ICSD#24276 (TiO_2-B). The anatase TiO_2 (Merck, p.a.) and Li_2CO_3 were mixed at mol ratio of 5:2 with zirconia balls as crushers with the weight ratio of material to zirconia balls at 1:30. The mixing process was done in a ball mill at 300 rpm for 2 hours and then continued at 480 rpm for 2 hours. The mixture was calcined at 800 °C for 4 hours to produce LTO-A and cooled at room temperature. Sample preparation was conducted for anatase TiO_2 TOSOH to produce LTO-B.

2.2 Analysis of Synthesized Materials

X-ray diffraction (XRD) analysis of the prepared sample was conducted with a Bruker D8 Advanced X-ray diffraction machine with Cu Kα1 radiation at λ = 1.542 nm, 50 kV in the 2Θ ranges between 10-80°. To study the sample's crystallinity and cell parameters, the diffraction data were refined using the Le Bail method with the RIETICA software application [22]. A scanning electron microscopy (SEM) test was conducted on an FEI Inspect s50 to investigate the surface morphology and estimate the particle size of the material. Pellets of TiO_2-A, TiO_2-B, LTO-A and LTO-B were prepared using a hydraulic press and then calcined at 500 °C for 2 hours. Impedance measurement was conducted using an LCR meter (LCR-8105G, 20Hz-5MHz) and the data were analyzed to calculate the electric conductivity. The impedance data were plotted as a Nyquist plot and the trendline was drawn according to the equation. The equation was used to determine cross points x_1 and x_2 between the curve and the *x*-axis. The distance between x_1 and x_2 is the resistance value.

2.3 Electrochemical Measurement

Anodes were constructed by coating an aqueous slurry containing composite powder (94.5 wt.%), acetylene black (1.00 wt.%), carboxy methyl cellulose and styrene butadiene rubber as binder (2.25 wt.%) onto a cooper foil with a thickness of 100 μm. The electrode was dried under vacuum at 120 °C for 24 hours and subsequently pressed by a lamination machine. The electrolyte was 1 M $LiPF_6$ in EC/DMC (1:1, v:v), while the commercial polypropylene wetted by $LiPF_6$ was used as the separator. The composite powder consisted of the synthesized LTO and commercial graphite at various mass ratios as listed in Table 1. The commercial $LiFePO_4$ coated onto the Al foil was used as the cathode. The cylindrical battery cell was assembled in an argon-filled glove box. The $LiFePO_4$/LTOG battery cells were charged/discharged between 2.5 and 3.65 V at a current of 100 mA and 1C (1C graphite = 372 mAg^{-1} and 1C LTO = 175 mAg^{-1}). The specific capacity of the LTO/graphite composite was calculated by using the entire mass of the LTO and the graphite.

Table 1 Composition of synthesized LTO and commercial graphite at various masses.

Cell name	Increasing LTO content to graphite (%wt)
1LTOG	1
5LTOG	5

3 Result and Discussion

The XRD patterns of the LTO-A and the LTO-B are depicted in Figure 1. The diffraction patterns show peaks that are in agreement with the standard diffraction of $Li_4Ti_5O_{12}$ (ICSD #84973), confirming that synthesis had successfully proceeded. The peaks in the LTO-A and LTO-B diffraction patterns are sharp, indicating high crystallinity. However, the unidentified peaks at 2Θ 20.4° and 41.3° indicate the presence of secondary phase with possibility phase of Li_2TiO_3 as a side product of LTO formation. The peaks at 2Θ of 69° and 70° were identified as anatase TiO_2 based on standard anatase diffraction ICSD #24276. Meanwhile, the peaks at 2Θ of 27.5° and 54° were identified as rutile TiO_2 based on standard rutile diffraction ICSD #16636. These rutile peaks may have resulted from a transformation of anatase to rutile at high reaction temperature. Therefore, four phases existed in the prepared LTO-A and LTO-B, i.e. $Li_4Ti_5O_{12}$, Li_2TiO_3, anatase TiO_2, and rutile TiO_2.

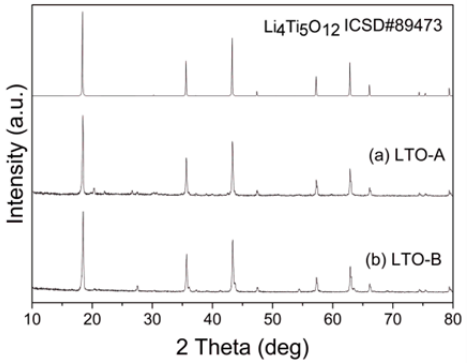

Figure 1 Diffraction patterns of (a) LTO-A and (b) LTO-B.

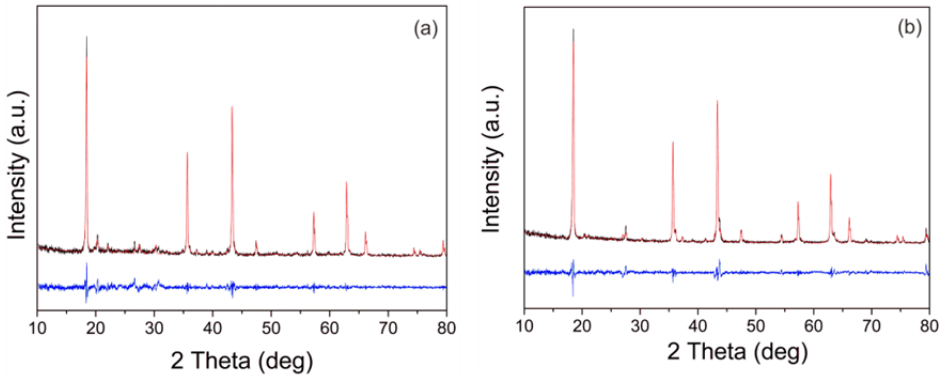

Figure 2 Le Bail plots of (a) LTO-A and (b) LTO-B obtained by calculation with 4 phases of $Li_4Ti_5O_{12}$, Li_2TiO_3, anatase TiO_2, and rutile TiO_2: experimental data, calculation data, difference between experimental data and calculation data.

The diffraction data were refined by the Le Bail method of which the results are shown in Figure 2. The refinement was carried out by inputting standard data of cubic crystal with space group *Fd-3m* ($Li_4Ti_5O_{12}$ ICSD# 84973), tetragonal crystal structure with space group *$I4_1/amd$* (anatase TiO_2 ICSD# 24276), tetragonal structure crystal with space group *$P4_2/mnm$* (rutile TiO_2 ICSD #16636), and monoclinic structure crystal and space group *C12/c1* (Li_2TiO_3 ICSD #15150).

Table 2 Cell parameters and crystal structure of prepared LTO-A and LTO-B.

Materials	**Cell parameters**	**$Li_4Ti_5O_{12}$ *Cubic Fd-3m***	**Li_2TiO_3 *Monoclinic C12/c1***	**TiO_2 anatase *Tetragonal $I4_1/amd$***	**TiO_2 rutile *Tetragonal $P4_2/mnm$***	**Crystal size (nm)**
LTO-A	*a* (Å)	8.351	5.091	3.839	4.624	48.289
	b (Å)	8.351	8.867	3.839	4.620	
	c (Å)	8.351	9.721	9.299	3.004	
	angle	α=β=γ= 90°	α= γ=90° β=99.521°	α=β=γ= 90°	α=β=γ= 90°	
	cell volume ($Å^3$)	582.486	432.255	137.073	64.239	
	Rp (%)	9.780				
	Rwp (%)	5.670				
LTO-B	*a* (Å)	8.378	5.113	3.860	4.604	38.547
	b (Å)	8.378	8.756	3.860	4.604	
	c (Å)	8.378	9.826	9.531	2.963	
	angle	α=β=γ= 90°	α= γ=90° β=100.936°	α=β=γ= 90°	α=β=γ= 90°	
	cell volume ($Å^3$)	588.044	431.952	142.050	62.801	
	Rp (%)	9.570				
	Rwp (%)	6.880				

Table 2 shows that the synthesized LTO-A and LTO-B contained cubic $Li_4Ti_5O_{12}$, monoclinic Li_2TiO_3, TiO_2 anatase, and TiO_2 rutile. The amount of Li_2TiO_3 monoclinic was still high due to the Li content being higher compared to that of Ti. The phase investigation confirmed that the solid state reaction did not produce 100% LTO powder, even though the reaction temperature was 800 °C for 4 hours. A longer reaction time may be required to ensure that the Li ions have sufficient time to go through the long diffusion path to TiO_2 structure [23]. Monoclinic Li_2TiO_3 is stable up to 1155 °C [24]. During synthesis, a solid reaction occurs between Li_2CO_3 and TiO_2 under high temperature.

The SEM image of the particle measurement result with MeasureIT analysis, as depicted in Figure 3, shows that the prepared LTO has micro size particles. The size and shape of the particles are not homogeneous, where some of the small particles seem to have agglomerated into a larger size. The SEM image analysis using MeasureIT (free edition) obtained particle sizes of LTO-A and LTO-B of

0.521 μm ± 0.180 μm and 0.533 μm ± 0.157 μm, respectively. Meanwhile, the LTO synthesized using $LiOH.H_2O$ and TiO_2 as starting materials produced agglomerates of particles with a size of around 25-34 μm [25], i.e. around 50 times larger than those produced by this research. Smaller particles are known to have an excellent rate discharge capability [26]. Therefore, the material with small-size particles is a promising electrode material due to the shorter distance for the Li+ ion diffusion and electron transfer [27]. It has been found that the Li^+ ion conductivity of $Li_4Ti_5O_{12}/Li_2TiO_3$ composite is 1.7 x 10^{-6} Scm^{-1}, which is higher than those of single $Li_4Ti_5O_{12}$ and single Li_2TiO_3, i.e. 5.7 x 10^{-7} Scm^{-1} and 2.5 x 10-7 Scm^{-1}, respectively [28]. An Li-rich interphase layer formed between $Li_4Ti_5O_{12}$ and Li_2TiO_3 may stabilize the crystal structure of the active material, resulting in enhanced cyclic stability [28].

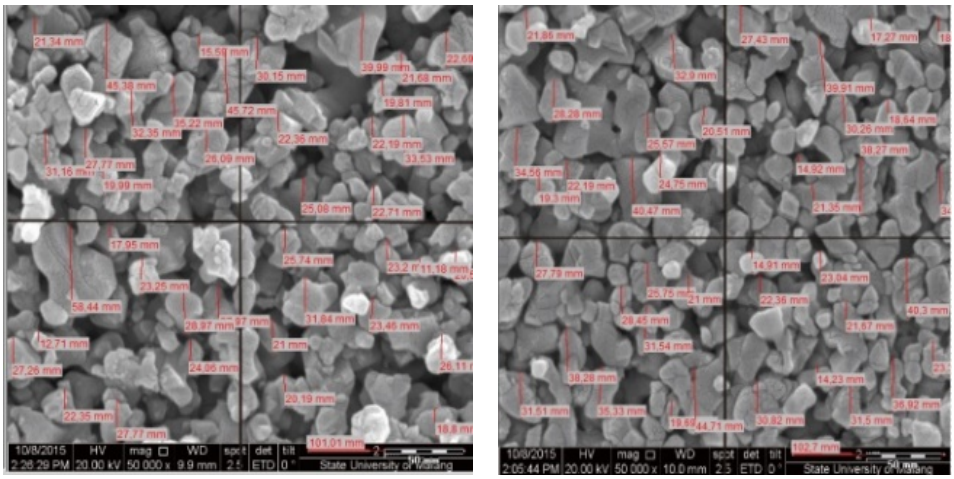

Figure 3 SEM images of (a) LTO-A and (b) LTO-B analyzed using MeasureIT sofware package.

The impedance plots, or Nyquist plots, of TiO_2-A, TiO_2-B, LTO-A, and LTO-B are shown in Figure 4. The impedance, or resistance value, is extracted by drawing the equation of the trendline and determines the cross points between the curve and the *x*-axis. The impedance values are listed in Table 3. The result shows that the impedance value of the LTO was lower than that of the TiO_2. This indicates that the ohmic resistance of the LTO is smaller than that of the TiO_2 when it is used as an electrode.

The conductivity values as calculated by Eq. (1) are also listed in Table 3. The result shows that the materials have ionic and electronic conductivity, confirming the ability to be used as electrode. The conductivity value is still small because a single electrode measurement was conducted without the presence of lithium ions, which are usually supplied by the electrolyte.

$$\sigma = \frac{l}{RxA} \tag{1}$$

In order to investigate the ability of a battery with an LTO/graphite mixture to be used as an anode, a single cell was constructed with LFP as the cathode and $LiPF_6$ as the electrolyte. Figure 5 shows the charge and discharge curves of the LFP/LTOG battery and the LFP/graphite battery within a potential window of 2.5-3.65 V at current 100 mA.

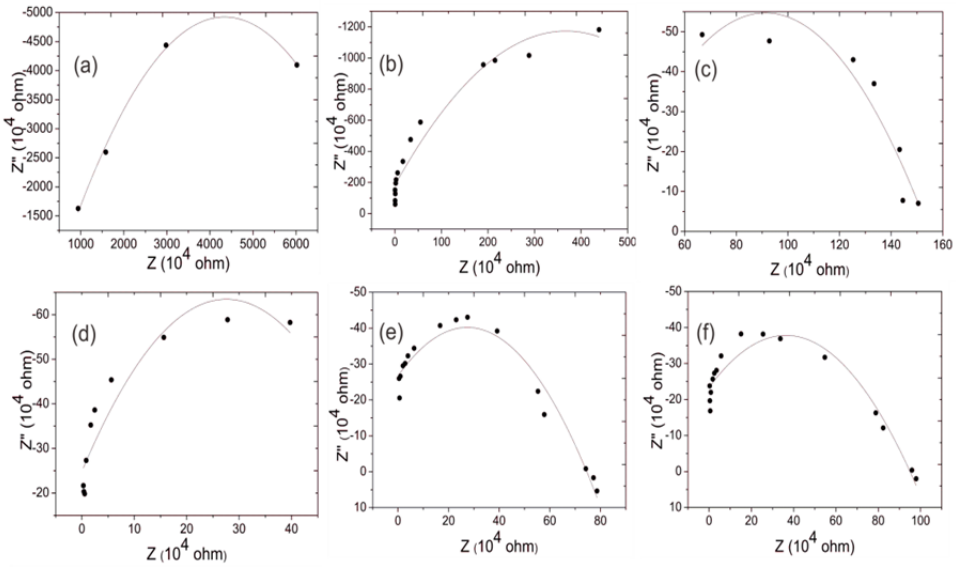

Figure 4 Nyquist plot materials of TiO_2-A: (a) 20 Hz-10 KHz; (b) 30 KHz-5 MHz, TiO_2-B; (c) 20 Hz-10 KHz; (d) 30 KHz-5 MHz; LTO-A (e) and LTO-B (f) at 20 Hz-5 MHz.

Table 3 Values of Impedance, Conductivity and Capacitance.

Materials	Impedance (10^7 ohm)	Capacitance (F)	Conductivity (10^{-7} S/cm)
TiO_2-A	8.770	$1.779\ 10^{-11}$ $1.104\ 10^{-11}$	0.217
TiO_2 -B	0.301	$1.270\ 10^{-10}$ $1.144\ 10^{-11}$	2.300
LTO-A	0.054	$1.157\ 10^{-11}$	9.284
LTO-B	0.085	$9.439\ 10^{-12}$	9.250

Figure 5 shows that, initially, the charge capacity is obviously larger than the discharge capacity, which may indicate that a side reaction such as the formation of solid electrolyte interface (SEI) may have occurred [29,30]. The presence of SEI on the electrode surface will prevent direct contact between the

Li and the solvent, making the Li dynamically stable in some organic solvents [31]. However, after the first cycle, the electrode reaction shows a high charge-discharge reversibility.

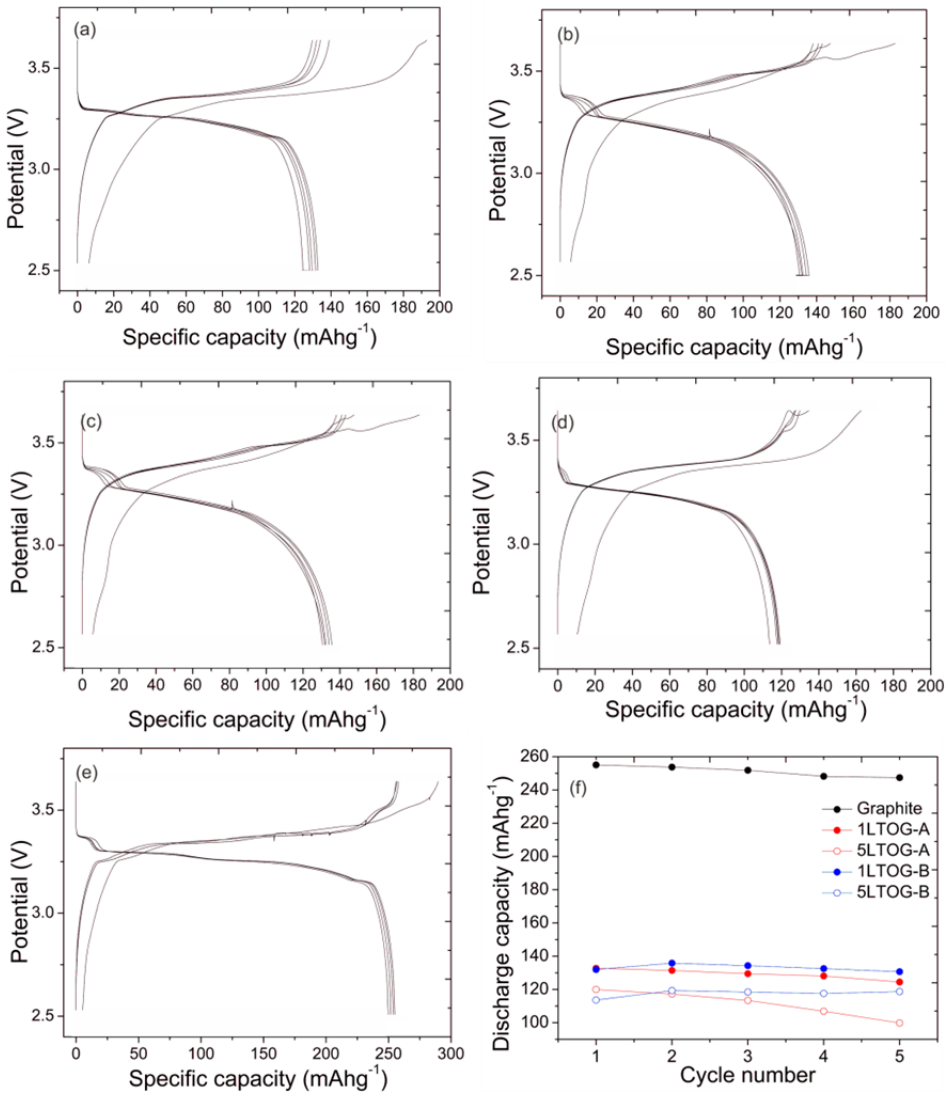

Figure 5 Galvanostatic charge-discharge voltage profiles of (a) LFP//1LTOG-A; (b) LFP//5LTOG-A; (c) LFP//1LTOG-B; (d) LFP//5LTOG-B; and (e) LFP//G, at a low current draw of 100 mA within a voltage range of 2.5-3.65 V; and (f) the discharge capacity profiles of all prepared battery cells.

Figure 5(c) and 5(e) show more dense curves than the other curves, indicating that the battery's stability is higher. Figure 5(f) shows that the discharge

capacity of the LFP/graphite under a current draw of 100 mA was 255.07 $mAhg^{-1}$, which is higher compared to LFP/1LTOG-A, LFP/5LTOG-A, LFP/1LTOG-B, and LFP/5LTOG-B, i.e. 132.75, 119.99, 131.99, and 113.64 $mAhg^{-1}$, respectively. It seems that the LTO addition even decreased the battery's specific capacity, theoretically, because the specific capacity of LTO is 175 $mAhg^{-1}$ while that of graphite is 372 $mAhg^{-1}$. The battery's performance data are listed in Table 4.

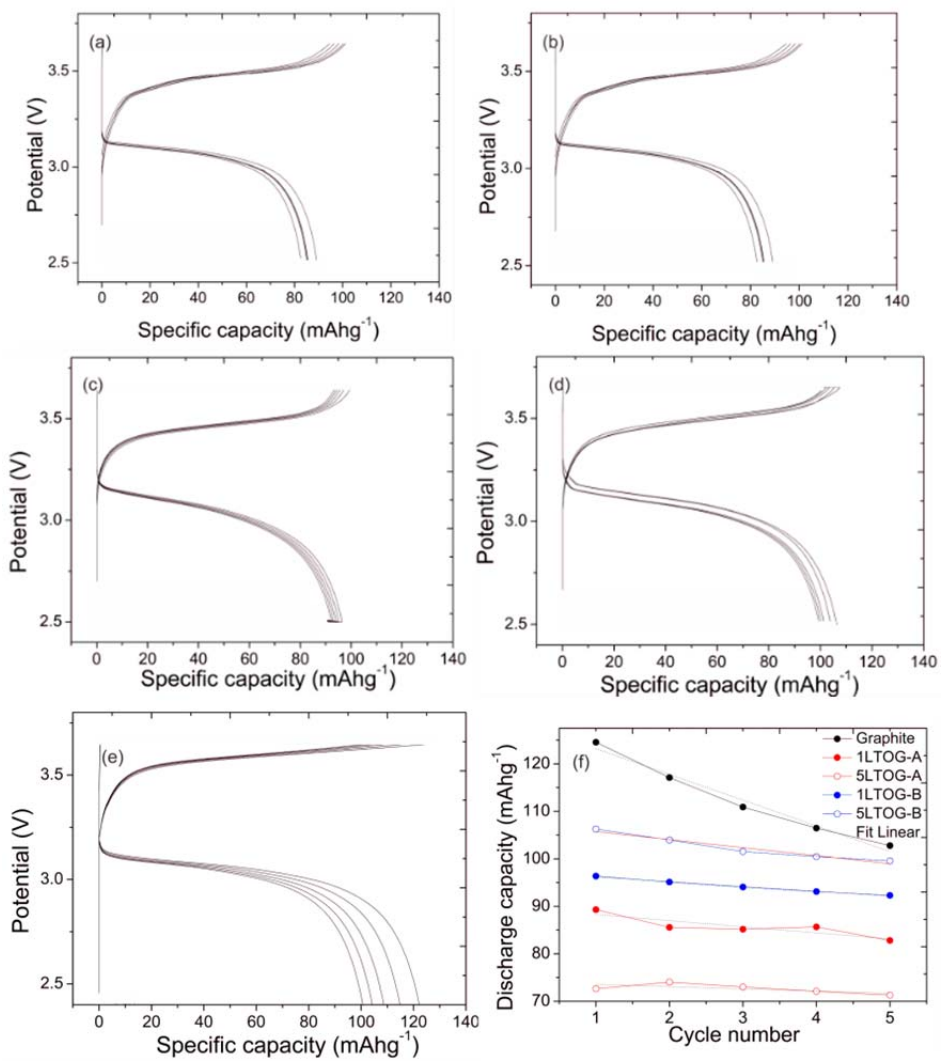

Figure 6 Galvanostatic charge-discharge voltage profiles of (a) LFP/1LTOG-A; (b) LFP/5LTOG-A; (c) LFP/1LTOG-B; (d) LFP/5LTOG-B; and (e) LFP/G at high current draw (1C) within a voltage range of 2.5-3.65 V; and (f) the discharge capacity profiles of all prepared battery cells.

To investigate the fast charging ability, in this research, battery performance was tested under 1C current draw. The results are depicted in Figure 6. Figures 6(a-d) show a more dense curve than Figure 6(e). This indicates that the presence of $Li_4Ti_5O_{12}$ increases the stability of the battery and allows it to still have good performance even after charge-discharge under high current. Figure 6(f) shows that the specific capacity of the LFP/G battery decreased faster and after 5 cycles the value was incomparable with that of the LFP/LTOG battery. This is shown by the slope value of LFP/G, i.e. 5.419 (Table 4). This indicates that the LFP/LTOG battery is more reliable for fast charging. The fast specific capacity reduction of the LFP/G battery is caused by the larger structural change in the graphite as shown by the increase of the cell parameters and the unit cell volume, which can reach up to 10% expansion [32].

Table 4 Result of charge and discharge at current 100 mA and 1C.

Cell Name	Cycle number	100 mA			1 C			
		Specific capacity (mAh/g)		Mean Coulombic Efficiency (%)	Specific capacity (mAh/g)		Mean Coulombic Efficiency (%)	Slope
		Charge	Discharge		Charge	Discharge		
LFP/ 1LTOG-A	1st	193.73	132.75	90.43	95.21	89.29	86.85	1.287
	5th	129.88	124.49		98.97	82.80		
LFP/ 5LTOG-A	1st	182.32	119.99	81.00	79.86	72.65	95.56	0.468
	5th	129.88	99.82		73.30	71.28		
LFP/ 1LTOG-B	1st	186.26	131.99	88.64	100.09	96.35	97.50	1.009
	5th	138.71	130.66		94.04	92.30		
LFP/ 5LTOG-B	1st	163.73	113.64	86.47	107.69	106.27	98.31	1.693
	5th	129.31	118.74		101.51	99.56		
LFP/G	1st	290.39	255.07	95.87	127.77	124.57	98.57	5.419
	5th	254.29	247.41		103.72	102.79		

Based on Table 4, the discharge capacities of the LFP/LTOG-B battery are higher than those of the LFP/LTOG-A battery. This is probably caused by the higher percentage, smaller particle size and higher conductivity of the LTO-B than the LTO-A, as can be seen in Tables 2 and 3. The smaller size of the crystal shortens the diffusion path in the intercalation and de-intercalation process of the Li^+ ions and also increases the contact area between the LTO and the electrolyte [23].

A rechargeable battery, for example a lithium ion battery, will become an electrolysis cell during the charging process and a voltaic cell during the discharging process following the prediction of the reaction using an LTO/graphite composite anode and an LFP cathode, as expressed in the following Eq. (2):

$$Li_4Ti_5O_{12} + C_6 + 4LiFePO_4 \underset{discharging}{\overset{charging}{\rightleftharpoons}} Li_7Ti_5O_{12} + LiC_6 + 4FePO_4 \quad (2)$$

4 Conclusion

Lithium titanate, LTO, consisting of $Li_4Ti_5O_{12}$ and monoclinic Li_2TiO_3, was synthesized by solid state reaction with TiO_2 powder and $LiCO_3$ powder as starting materials. The LTO/graphite mix powder electrodes showed good performance when it was used as anode material for a lithium ion battery.

Acknowledgements

This research was part of Hibah Mandatory 2017 funded by PNBP Sebelas Maret University, Contract No. 623/UN27.21/PP/2017, and also part of USAID Sustainable Higher Education Research Alliances (USAID SHERA), Prime Award No. AID-497-A16-0004, Subaward No. IIE00000078-ITB-1. The authors express their gratitude for the support.

References

[1] Yang, Z., Zhang, J., Kintner-Meyer, M.C.W., Lu, X., Choi, D. & Lemmon, J.P., *Electrochemical Energy Storage for Green Grid*, Chemical Reviews, **111**(5), pp. 3577-3613, 2015.

[2] Rastler, D., *Electricity Energy Storage Technology Options*, Technical Report 1020676, Electric Power Research Institute, California, Dec. 2010.

[3] Goodenough, J.B. & Kim, Y., *Challenges for Rechargeable Li Batteries*, Chemistry of Materials, **22**(3), pp. 587-603, 2010.

[4] Nitta, N., Wu, F., Lee, J.T. & Yushin, G., *Li-ion Battery Materials: Present and Future*, Materials Today, **18**(5), pp. 252-264, 2015.

[5] Chen, J., *Recent Progress in Advanced Materials for Lithium Ion Batteries*, Materials, **6**, pp. 156-183, 2013.

[6] Goriparti, S., Miele, E., De Angelis, F., Di Fabrizio, D., Proietti Zaccaria, R. & Capiglia, C., *Review on Recent Progress of Nanostructured Anode Materials for Li-Ion Batteries*, Journal of Power Sources, **257**, pp. 421-443, 2014.

[7] Wenelska, K., Ottmann, A., Schneider, P., Thauer, E., Klingeler, R. & Mijowska, E., *Hollow Carbon Sphere/Metal Oxide Nanocomposites Anodes for Lithium-Ion Batteries*, Energy, **103**, pp. 100-106, 2016.

[8] Eftekhari, A., *Low Voltage Anode Materials for Lithium-Ion Batteries*, Energy Storage Materials, **7**, pp. 157-180, 2017.

[9] Zhang, H., Liu, Y., Wang, T., Yang, Y., Shi, S. & Yang, G., *Li_2ZrO_3-Coated $Li_4Ti_5O_{12}$ with Nanoscale Interface for High Performance Lithium-Ion Batteries*, Applied Surface Science, **368**, pp. 56-62, 2016.

[10] Ding, Y., Li, G.R., Xiao, C.W. & Gao, X.P., *Insight into Effects of Graphene in $Li_4Ti_5O_{12}$/Carbon Composite with High Rate Capability as Anode Materials for Lithium Ion Battery*, Electrochimica Acta, **102**, pp. 282-289, 2013.

[11] Hu, X., Huai, Y., Lin, Y., Suo, J. & Deng, Z., *A ($LiFePO_4$-AC)/$Li_4Ti_5O_{12}$ Hybride Battery Capacitor*, Journal of The Electrochemical Society, **154**(11), pp. A1026-A1030, 2007.

[12] Chen, C., Agrawal, R. & Wang, C., *High Performance $Li_4Ti_5O_{12}$/Si Composite Anodes for Li-Ion Batteries*, Nanomaterials, **5**(3), pp. 1469-1480, 2015.

[13] Wang, Y.Q., Gu, L., Guo, Y.G., Li, H., He, X.Q., Sukimoto, S., Ikuhara, Y. & Wan, L.J., *Rutile-TiO_2 Nanocoating for a High-Rate $Li_4Ti_5O_{12}$ Anode Lithium-Ion Battery*, Journal of The American Chemical Society, **134**(18), pp. 7874-7879, 2012.

[14] Zhao, Y., Pang, S., Zhang, C., Zhang, Q., Gu, L., Zhou, X., Li, G. & Cui, G., *Nitridated Mesoporous $Li_4Ti_5O_{12}$ Spheres for High-Rate Lithium-Ion Batteries Anode Material*, Journal Solid State Electrochemical, **17**(5), pp. 1479-1485, 2013.

[15] Sun, X., Radovanovic, P.V. & Cui, B., *Advances in Spinel $Li_4Ti_5O_{12}$ Anode Materials for Lithium-Ion Batteries*, New Journal of Chemistry, **39**(1), pp. 38-63, 2015.

[16] Syahrial, A.Z., Priyono, B., Yuwono, A.H., Kartini, E., Jodi, H. & Johansyah, *Synthesis of Lithium Titanante ($Li_4Ti_5O_{12}$) by Addition of Excess Lithium Carbonate (Li_2CO_3) in Titanium Dioxide (TiO_2) Xerogel*, International Journal of Technology, **7**(3), pp. 392-400, 2016.

[17] Valvo, M., Liivat, A., Eriksson, H., Tai, C.W. & Edström, K., *Iron-Based Electrodes Meet Water-Based Preparation, Fluorine-Free Electrolyte and Binder: A Chance for More Sustainable Lithium-Ion Batteries?*, ChemSusChem, **10**(11), pp. 2431-2448, 2017.

[18] Choi, D., Wang, D., Viswanathan, V.V., Bae, I.T., Wang, W., Nie, Z., Zhang, J.G., Graff, G.L., Liu, J., Yang, Z. & Duong, T., *Li-Ion Batteries from $LiFePO_4$ Cathode and Anatase/Graphene Composite Anode for Stationary Energy Storage*, Electrochemistry Communications, **12**(3), pp. 378-381, 2010.

[19] Wang, W., Choi, D. & Yang, Z., *Li-Ion Battery with $LiFePO_4$ Cathode and $Li_4Ti_5O_{12}$ for Stationary Energy Storage*, Metallurgical and Materials Transaction A, **44A**(1), pp. 21-25, 2013.

[20] Cheng, Q., Liang, J., Zhu, Y., Si, L., Guo, C. & Qian, Y., *Bulk $Ti_2Nb_{10}O_{12}$ as Long-life and High-power Li-ion Battery Anodes*, Journal of Materials Chemistry A, **41**, pp. 17258-17262, 2014.

[21] Veljkovi, I., Poleti, D., Karanovi, L., Zduji, M. & and Brankovi, G., *Solid State Synthesis of Extra Pahse-Pure $Li_4Ti_5O_{12}$ Spinel*, Science of Sintering, **43**, pp. 343-351, 2011.

[22] Peterson, V.K., *Lattice Parameter Measurement using Le Bail versus Structural (Rietveld) Refinement: A Caution for Complex, Low Symmetry Systems*, Power Diffraction, **20**(1), pp. 14-17, 2005.

[23] Shin, J., Hong, C. & Yoon, D., *Effects of TiO_2 Starting Materials on the Solid-State Formation of $Li_4Ti_5O_{12}$*, Journal of the American Ceramic Society, **7**, pp. 1-7, 2012.

[24] Kleykamp, H., *Phase Equilibria in the Li-Ti-O System and Physical Properties of Li_2TiO_3*, Fusion Engineering Design, **61-62**, pp. 361-366, 2002.

[25] Priyono, S., Primasari, R.D., Saptari, S.A. & Prihandoko, B., *Synthesized $Li_4Ti_5O_{12}$ from Technical Grade Raw Material by Excess $LiOH.H_2O$ as Anode for Lithium Ion Battery*, Journal of Physics: Conference Series, **87**, pp. 1-6, 2017.

[26] Lai, C., Wu, Z., Zhu, Y., Wu, Q., Li, L. & Wang, C., *Ball-milling assisted Solid-State Reaction Synthesis of Mesoporous $Li_4Ti_5O_{12}$ for Lithium-Ion Batteries Anode*, Journal of Power Sources, **226**, pp. 71-74, 2013.

[27] Sandhya, C.P., John, B. & Gouri, C., *Lithium Titanate as Anode Material for Lithium-Ion Cells: A review*, Ionics, **20**(5), pp. 601-620, 2014.

[28] Wang, Y., Zhou, A., Dai, X., Feng, L., Lie, J. & Li, J., *Solid-State Synthesis of Submicron-Sized $Li_4Ti_5O_{12}/Li_2TiO_3$ Composites with Rich Grain Boundaries for Lithium Ion Batteries*, Journal of Power Sources, **266**, pp. 114-120, 2014.

[29] Yang, C., Hu, H., Lin, S.J. & Chien, W., *Electrochemical Performance of V-Doped Spinel $Li_4Ti_5O_{12}/C$ Composite Anode in Li-Half and $Li_4Ti_5O_{12}/LiFePO_4$-Full Cell*, Journal Power Sources, **258**(15), pp. 424-433, 2014.

[30] Dong, Y., Zhao, Y., Duan, H. & Huang, J., *Electrochemical Performance and Lithium-Ion Insertion/Extraction Mechanism Studies of the Novel Li_2ZrO_3 Anode Materials*, Electrochimica Acta, **161**, pp. 219-225, 2015.

[31] Cheng, X., Zhang, R., Zhao, C., Wei, F., Zhang, J. & Zhang, Q., *A Review of Solid Electrolyte Interphases on Lithium Metal Anode*, Advanced Science, **3**(3), pp. 1-20, 2016.

[32] Qi, Y. & Harris, S.J., *In Situ Observation of Strain during Lithiation of a Graphite Electrode*, Journal of The Electrochemical Society, **157**(6), pp. A741-A747, 2010.